Pergamon

Int. J. Heat Mass Transfer. Vol. 40, No. 6, pp. 1291–1302, 1997

0017-9310/97 $17.00+0.00

PII: S0017-9310(96)00208-6

A hydrodynamic critical heat flux model for saturated pool boiling on a downward facing curved heating surface

F. B. CHEUNG and K. H. HADDAD
Department of Mechanical Engineering, Pennsylvania State University, University Park, PA 16802, U.S.A.

(*Received* 20 *January* 1996 *and in final form* 3 *June* 1996)

Abstract—A theoretical model is developed to predict the critical heat flux (CHF) limit for saturated pool boiling on the outer surface of a heated hemispherical vessel. The model considers the existence of a micro-layer underneath an elongated vapor slug on a downward facing curved heating surface. The micro-layer is treated as a thin liquid film with numerous micro-vapor jets penetrating it. The micro-jets have the characteristic size dictated by Helmholtz instability. Local dryout is considered to occur when the supply of fresh liquid from the two-phase boundary layer to the micro-layer is not sufficient to prevent depletion of the liquid film by boiling. A boundary layer analysis, treating the two-phase motion as an external buoyancy-driven flow, is performed to determine the liquid supply rate and thus the local critical heat flux. The model provides a clear physical explanation for the spatial variation of the CHF observed in experiments and for the weak dependence of the CHF data on the physical size of the vessel. Copyright © 1996 Elsevier Science Ltd.

INTRODUCTION

In recent years, the concept of external passive cooling of core melt in the lower head of a reactor vessel by cavity flooding, has been considered a viable strategy for severe accident management. In this concept, water is made available on the bottom side of the reactor vessel by flooding the reactor cavity during a severe core-meltdown accident. As the lower head is heated by the pool of core melt resulting from the accident, the decay heat generated in the melt is removed from the external bottom surface of the reactor vessel by boiling of the water in the flooded cavity. If this mode of passive cooling is effective in the post-accident stage, then thermal failure of the reactor vessel can be prevented and the radioactive core melt can be retained within the reactor vessel. The feasibility of the cavity-flooding concept depends, however, heavily on the critical heat flux distribution on the external bottom surface of the reactor vessel.

For the case in which the critical heat flux (CHF) is higher than the local heat flux from the core melt, nucleate boiling will be the prevailing mode of heat transfer and the vessel wall can be maintained well below the failure temperature of the vessel. On the other hand, if the local heat flux from the core melt exceeds the CHF limit, then transition to film boiling might occur and the integrity of the reactor lower head could be severely jeopardized. Note that as vapor bubbles grow and depart from the heating surface, they tend to flow upward along the external bottom surface of the vessel. This results in a two-phase liquid–vapor boundary layer, driven by buoyancy under the influence of gravity, along the downward facing curved heating surface. The formation of the two-phase boundary layer, which is a direct consequence of vapor generation, may in turn affect the boiling process and the local CHF limit. In spite of its practical importance, very little is known about the critical heat flux on a downward facing curved heating surface with the presence of a two-phase boundary layer.

The mechanism responsible for the occurrence of CHF in pool boiling has been the subject of extensive investigation and debate in the past several decades [1, 2]. Kutateladze [3] was the first to propose the analogy between the flooding phenomenon and the CHF condition. This analogy was first mentioned by Bonilla and Perry in 1941 as reported by Zuber [4], but it appears that Kutateladze was the first to pursue the idea. He used dimensional analysis to derive an expression for the critical heat flux.

Zuber [4] developed a hydrodynamic CHF model based on Taylor wave motion and Helmholtz instability. He assumed burnout to be attained when the interface of the large vapor columns leaving the surface became Helmholtz unstable. The vapor columns were separated from each other by a distance equal to the most dangerous Taylor wavelength. An expression for the critical heat flux similar to the one proposed by Kutateladze [3] was obtained by Zuber [4]. Some refinements of Zuber's model were made by Lienhard and Dhir [5], which resulted in a slightly different value for the constant coefficient.

NOMENCLATURE

A_v	surface area occupied by the micro-vapor jets underneath an elongated vapor slug
A_w	total heating surface area underneath an elongated vapor slug
B	universal constant, equation (17)
E_0	entrainment coefficient, equation (42)
h_{fg}	latent heat of vaporization
j_ℓ	liquid entrainment velocity, equation (20)
J_ℓ	dimensionless liquid entrainment velocity, equation (30)
L_b	dimensionless length scale ratio, equation (31)
q''_{CHF}	local critical heat flux at any location θ
Q_{CHF}	dimensionless local critical heat flux, equation (23a)
q''_{NB}	nucleate boiling heat flux at any location θ
R	radius of the hemispherical vessel
u_g	axial velocity of the vapor phase in the two-phase boundary layer
u_ℓ	axial velocity of the liquid phase in the two-phase boundary layer
U_g	dimensionless axial velocity of the vapor phase, equation (23c)
U_ℓ	dimensionless axial velocity of the liquid phase, equation (23d)
v_g	vertical velocity of the micro-vapor jets in the micro-layer, equation (1)
v_ℓ	vertical velocity of the liquid film in the micro-layer, equation (2).

Greek symbols

α	local void fraction of the two-phase boundary layer
δ	local thickness of the two-phase boundary layer
δ_m	thickness of the micro-layer under an elongated vapor slug, equation (9)
Δ	dimensionless local boundary layer thickness, equation (23b)
λ_H	Helmholtz wavelength, equation (4)
ρ_g	vapor density
ρ_ℓ	liquid density
σ	surface tension
θ	angular position from the bottom center of the hemispherical vessel.

Lienhard and Hasan [6] used the mechanical energy stability criterion to predict the CHF in pool boiling. They considered the boiling system to be in stable equilibrium when the change in the system energy was equal to or less than zero. For nucleate boiling, this implies that the mechanism of vapor removal remains stable as long as the net mechanical energy transfer to the system is negative. Violation of this condition marks the occurrence of CHF. Using this principle, Leinhard and Hasan were able to show that the results of their analysis were consistent with Zuber's model. They also showed that their model eliminated the need for information on the Helmholtz unstable wavelength. However, this was replaced by the need for information on the bubble departure diameter corresponding to the breakup of the vapor column.

Haramura and Katto [7] postulated that a liquid film existed underneath each vapor bubble growing on the heating surface. The vapor bubble hovered over a number of small jets that supplied the bubble with vapor mass, leading to a timely growth of the bubble until it was pulled upward away from the surface by buoyancy. The bubbles were arranged in a rectangular array with a spacing equal to the most dangerous Taylor wavelengths whereas the liquid film thickness was one-fourth of the Helmholtz wavelength. Burnout was assumed to take place when the liquid film underneath the vapor bubble evaporated completely before the departure of the bubble. An expression similar to the one by Zuber [4] was derived for the CHF, with the constant coefficient being replaced by a function of the area ratio of the vapor jets to the heating surface.

In all the existing CHF models, the critical heat flux was treated constant and uniform over the entire heating surface. Thus far, no attempt has ever been made to predict the spatial variation of the critical heat flux. While the assumption of a uniform critical heat flux is a good approximation for upward facing surfaces, it is not a valid assumption for downward facing surfaces. In the latter case, a two-phase boundary layer flow is likely to be induced by the boiling process owing to the downward facing orientation of the heating surface. With the development of a boundary layer flow, the local critical heat flux could be substantially modified by the flow, thus leading to a significant spatial variation of the CHF values along the heating surface in the flow direction. Conceivably, none of the existing CHF models is applicable to pool boiling on a downward facing heating surface. It should also be noted that correlations for the maximum pool boiling heat flux have been restricted to the geometrically averaged CHF value for the heating objects, as summarized by Carey [2]. The reported data on the spatial variation of CHF are limited to those by Cheung and Haddad [8, 9], Haddad, Liu and

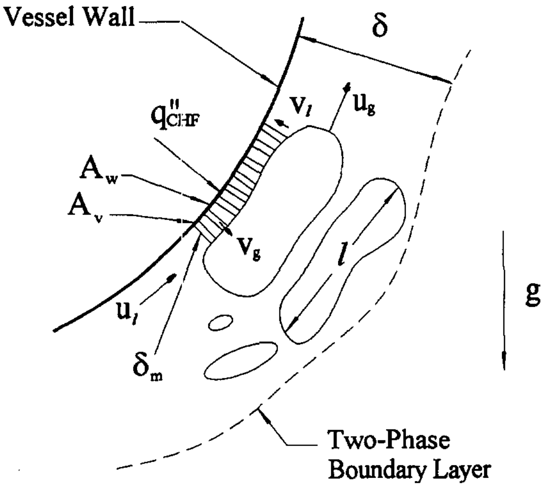

Fig. 1. Schematic of the micro-layer underneath an elongated vapor slug.

Cheung [10], El-Genk and Glebov [11], and Theofanous *et al.* [12].

BACKGROUND

Subscale boundary layer boiling (SBLB) experiments were recently conducted by Cheung and Haddad [8, 9] and Haddad *et al.* [10] to observe the critical heat flux phenomenon and the two-phase boundary layer flow on the outer surface of a heated hemispherical vessel submerged in a large pool of water. In their experiments, the local wall heat flux was varied from 0.05 MW m^{-2} up to the vicinity of the local CHF limit. At these high-heat-flux levels, a cyclic vapor ejection process was clearly observed. Large and elongated vapor masses or slugs, being squeezed up against the vessel wall by the local buoyancy force, were found to grow periodically on the downward facing curved heating surface. They were then ejected violently upward in all directions. The ejected vapor masses carried away the local vapor bubbles but tended to by-pass those large vapor slugs growing on the heating surface in the downstream locations, resulting in a two-phase boundary layer flow. A close-up view of the vapor slugs revealed the existence of a thin liquid film, i.e., a micro-layer, underneath each elongated vapor slug. The small vapor masses that were generated by boiling at numerous discrete locations on the heating surface were fed in a continuous manner to the large vapor slug through the liquid film in the micro-layer. These small vapor masses had the shape of micro-vapor jets similar to those depicted in Fig. 1. Apparently, it was the thin liquid film underneath the large vapor slug that prevented local dryout of the heating surface from occurring.

Near the local CHF limit, the characteristic frequency of the vapor ejection cycle was found to be approximately 4 Hz. Thus the cycle duration was about 0.25 s. This value was similar to the one observed by Chu, Bentz and Simpson [13] on the outer surface of a heated torispherical vessel. Over 90% of this duration, the heating surface was covered by the vapor slugs. The waiting period was less than 10% of the cycle duration. High-speed photographic records indicated that the statistically averaged void fraction was very close to 0.915 as the CHF limit was approached. The overall two-phase boundary layer flow configuration was similar to the one depicted in Fig. 2. At the bottom center of the vessel, only a single large elongated vapor mass having an aspect ratio (i.e. length-to-thickness ratio) of approximately four, was present in the local boundary layer region. However, in the downstream locations, two or three large vapor slugs could be present in the local boundary layer region at the same time. Upon departure, a vapor slug tended to flow around those that were growing on the heating surface in the downstream locations. The local boundary layer thickness increased considerably from the bottom center to the upper edge of the heated vessel. No apparent changes in the vapor dynamics and cyclic ejection process were observed as the CHF point was attained. The vapor/liquid morphology and the local flow behavior were essentially the same throughout the high-heat-flux regime up to the CHF point, although the characteristic frequency of the vapor ejection cycle tended to increase with the heat flux level. Clearly, the CHF point is a continuation of the nucleate boiling region and simply represents the upper limit of the high-heat-flux regime. Throughout the entire high-heat-flux region including the CHF point, nucleate boiling is subject to Helmholtz instability.

THEORETICAL MODELING

Most existing hydrodynamic CHF models were developed primarily for upward facing surfaces. The critical heat flux was treated as a peculiar point that was different radically from the nucleate boiling regime. Helmholtz instability was assumed to act on the CHF point only, causing a sudden collapse of the vapor removal path. The validity of these conventional models for downward facing surfaces is highly skeptical. The nucleate boiling phenomenon on the outer surface of a heated hemispherical vessel observed by Cheung and Haddad [8, 9] and Haddad *et al.* [10] clearly indicated that throughout the entire high heat flux regime, nucleate boiling was subject to Helmholtz instability with cyclic ejection of large elongated vapor masses or slugs from the downward facing curved heating surface. Underneath each vapor slug was a micro-layer consisting of a continuous liquid film with numerous micro-vapor jets penetrating it. The size of the micro-jets was dictated by Helmholtz instability. The CHF limit was reached as a result of insufficient supply of liquid from the two-phase boundary layer to the micro-layer, leading to depletion of the liquid film, i.e. local dryout of the heating surface. In view of this, the CHF point is a

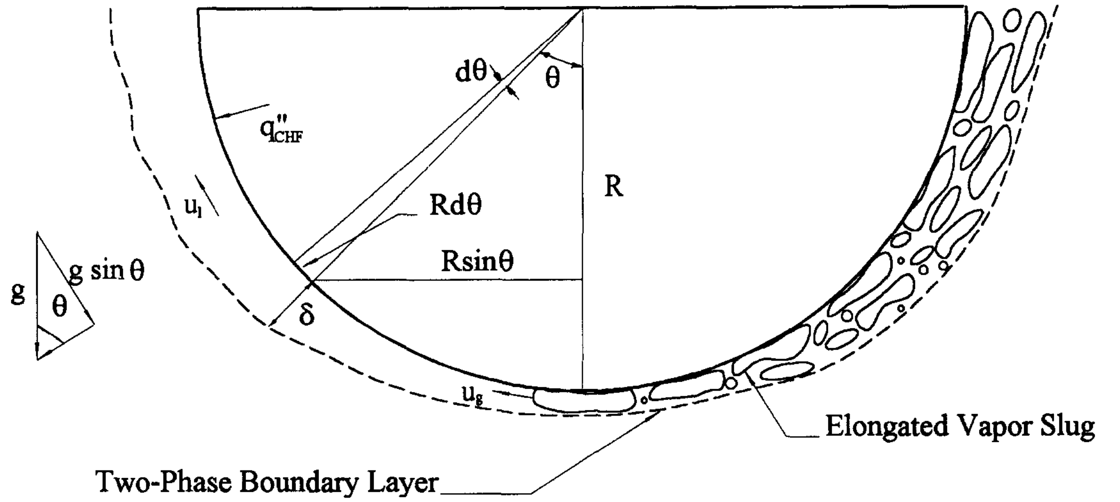

Fig. 2. Configuration of the two-phase boundary layer on the outer surface of a heated hemispherical vessel.

continuation of the nucleate boiling region in the high-heat-flux regime. This important new feature is employed in this study to develop an advanced hydrodynamic CHF model for pool boiling on a downward facing hemispherical heating surface.

Behavior of the micro-layer

Figure 1 shows schematically the configuration of a micro-layer underneath an elongated vapor slug growing on a downward facing curved heating surface. The micro-layer consists of a continuous liquid film with numerous micro-vapor jets or stems penetrating it. The thickness of the liquid film, δ_m is the same as the length of the vapor stems. Under steady-state saturated boiling conditions, the mass flow rate of the vapor jets must be equal to the local rate of nucleate boiling, i.e.

$$\rho_g v_g A_v = q''_{NB} A_w / h_{fg} \quad \text{or } v_g = \frac{q''_{NB}}{\rho_g h_{fg}} \frac{A_w}{A_v} \tag{1}$$

where ρ_g is the vapor density, v_g the vapor jet velocity, A_v the surface area occupied by all the vapor jets, A_w the total heating area underneath the elongated vapor slug, q''_{NB} the local nucleate boiling heat flux and h_{fg} the latent heat of vaporization. To satisfy continuity, the rate of liquid depletion of the micro-layer must be given by

$$\rho_\ell v_\ell (A_w - A_v) = q''_{NB} A_w / h_{fg} \quad \text{or } v_\ell = \frac{q''_{NB}}{\rho_\ell h_{fg}} \frac{A_w}{A_w - A_v} \tag{2}$$

where ρ_ℓ is the liquid density and v_ℓ the velocity of the liquid in the micro-layer flowing vertically toward the heating surface.

According to the Helmholtz instability [2], the relative velocity between the vapor jets and the liquid film in the micro-layer is given by

$$|v_g - v_\ell| = \left[\frac{2\pi\sigma(\rho_\ell + \rho_g)}{\lambda_H \rho_\ell \rho_g}\right]^{1/2} \tag{3}$$

where σ is the surface tension and λ_H the Helmholtz wavelength. Rearranging the above equation, the Helmholtz wavelength can be expressed in terms of the relative velocity by

$$\lambda_H = \frac{2\pi\sigma}{\rho_g}\left(1 + \frac{\rho_g}{\rho_\ell}\right)|v_g - v_\ell|^{-2}. \tag{4}$$

For the vapor jets to be hydrodynamically stable within the liquid film, the length of the jets should remain smaller than the Helmholtz wavelength. This implies that

$$\delta_m < \lambda_H \quad \text{or } \delta_m = C_1 \lambda_H \tag{5}$$

where C_1 is a proportionality constant having a value less than unity.

Assuming a value of 0.25 for C_1, Haramura and Katto [7] have shown that the micro-layer area ratio is a function of the density ratio of the fluid satisfying the following form:

$$\frac{A_v}{A_w} = 0.0584\left(\frac{\rho_g}{\rho_\ell}\right)^{0.2}. \tag{6}$$

The above expression was found to match the conventional pool boiling data for water and R-113 very nicely, independent of the configuration of the heating surface. However, the liquid film thickness so predicted ($\delta_m \sim 0.056$ mm) was almost a factor of two smaller than the measured value ($\delta_m \sim 0.12$ mm). This discrepancy was evidently due to the assumption of $C_1 = 0.25$ which was somewhat arbitrary. To be general, the exact value of C_1 will not be assumed in this study and the following expression will be employed in place of equation (6)

$$\frac{A_v}{A_w} = C_2\left(\frac{\rho_g}{\rho_\ell}\right)^{0.2} \quad (7)$$

where C_2 is treated as an unknown constant having a value much less than unity.

For most fluids at moderate pressures, the density ratio is usually much less than unity, i.e. $(\rho_g/\rho_\ell) \ll 1$. It follows from equations (1), (2) and (7) that

$$\frac{v_\ell}{v_g} = \frac{C_2(\rho_g/\rho_\ell)^{1.2}}{1-C_2(\rho_g/\rho_\ell)^{0.2}} \ll 1 \quad (8)$$

The above inquality is valid since both C_2 and ρ_g/ρ_ℓ are much less than unity. Hence the relative velocity between the vapor jets and the liquid film is essentially the same as the vapor jet velocity itself. Combination of equations (1), (4), (5) and (7) gives

$$\delta_m = C_3\sigma\rho_g\left(1+\frac{\rho_g}{\rho_\ell}\right)\left(\frac{\rho_g}{\rho_\ell}\right)^{0.4}\left(\frac{h_{fg}}{q''_{NB}}\right)^2 \quad (9)$$

where C_3 is a new constant equal to $2\pi C_1 C_2^2$.

Occurrence of the local CHF

Referring to Fig. 1, the local rate of liquid supply, $\dot{m}_s$, from the two-phase boundary layer to the micro-layer is given by

$$\dot{m}_s = \rho_\ell u_\ell A_m \quad (10)$$

where u_ℓ is the local liquid velocity in the two phase boundary layer and A_m the net local flow area across the micro-layer. On the other hand, the local rate of depletion, $\dot{m}_d$, of the liquid film is given by

$$\dot{m}_d = q'_{NB}A_w/h_{fg} \quad (11)$$

where A_w is the heating surface area underneath the elongated vapor slug. Local dryout of the liquid film is considered to occur when the local rate of liquid supply becomes smaller than the local rate of liquid depletion. In other words, the local critical heat flux limit is reached when the liquid supply from the two-phase boundary layer to the micro-layer is not sufficient to prevent local boil-dry of the liquid film. From equations (10) and (11), an expression for the local critical heat flux, q''_{CHF}, can be obtained by setting $\dot{m}_s$ equal to $\dot{m}_d$ and q''_{NB} equal to q''_{CHF}, i.e.

$$q''_{CHF} = \rho_\ell h_{fg} u_\ell\left(\frac{A_m}{A_w}\right) \quad (12)$$

where A_m is now the net flow area across the micro-layer at the local CHF point.

Assuming the characteristic length of the vapor slug to be ℓ, the net flow area A_m and the heating surface area A_w can be expressed by

$$A_m \sim (\delta_m)_{CHF}\ell \quad \text{and} \quad A_w \sim \ell^2 \quad (13)$$

where $(\delta_m)_{CHF}$ is the thickness of the micro-layer at the local CHF point, i.e. at q''_{CHF}. From the two-phase boundary layer flow observations by Cheung and Haddad [8, 9], the characteristic length ℓ, is found to be proportional to the local two-phase boundary layer thickness, δ_0, in the bottom center region, i.e.

$$\ell = C_4\delta_0 \quad (14)$$

where C_4 is a constant having a value very close to four along the curved heating surface. Substituting equations (13) and (14) into equation (12), the following expression is obtained for the local critical heat flux:

$$q''_{CHF} = \rho_\ell h_{fg} u_\ell(\delta_m)_{CHF}/C_4\delta_0 \quad (15)$$

where additional proportionality constants from equation (13) have been absorbed in C_4.

As discussed earlier, the CHF point is a continuation of the nucleate boiling region in the high-heat-flux regime. Helmholtz instability is acting upon the micro-layer throughout the entire high-heat-flux nucleate boiling regime including the CHF point. Hence, equation (9) should be applicable to the CHF limit. By setting q''_{NB} equal to q''_{CHF}, equation (9) becomes

$$(\delta_m)_{CHF} = C_3\sigma\rho_g\left(1+\frac{\rho_g}{\rho_\ell}\right)\left(\frac{\rho_g}{\rho_\ell}\right)^{0.4}\left(\frac{h_{fg}}{q''_{CHF}}\right)^2. \quad (16)$$

Substitution of equation (16) into equation (15) gives

$$q''_{CHF} = B\rho_g h_{fg}\left[\frac{\sigma u_\ell}{\rho_\ell\delta_0}\left(1+\frac{\rho_g}{\rho_\ell}\right)\left(\frac{\rho_g}{\rho_\ell}\right)^{-1.6}\right]^{1/3} \quad (17)$$

where $B = (C_3/C_4)^{1/3}$ is a new constant. Evidently, the local critical heat flux varies according to the 1/3 power of the local liquid velocity. This local flow quantity, which is expected to increase significantly along the heating surface in the flow direction, will be determined by treating the two-phase boundary layer motion as an external buoyancy-driven flow.

It should be noted that the dependence of the CHF limit on the local liquid velocity in the two-phase boundary layer given by equation (17) is similar to the one observed for forced convection boiling of the external flow type where the critical heat flux is proportional to the 1/3 power of the mass velocity of the ambient liquid flow [7]. This similarity clearly shows the rather unconventional features associated with the present boundary-layer-type pool boiling process. Although it is a pool boiling phenomenon, the process exhibits flow boiling characteristics. Physically, this is because of the formation of the two-phase boundary layer along the downward facing curved heating surface in the present pool boiling case. Owing to the effect of the two-phase boundary layer, the CHF phenomenon at a given downstream location exhibits the same characteristic behavior as the one observed for external flow boiling.

Two-phase boundary layer analysis

Figure 2 depicts the external buoyancy-driven two-phase boundary layer flow on the outer surface of a hemispherical vessel. The vessel has a radius R and is heated from inside. The ambient liquid is saturated and quiescent, and the boundary layer motion is induced entirely by pool boiling of the saturated liquid on the vessel outer surface. To describe the boundary layer variables, an axisymmetric spherical coordinate system is employed. The radial and angular positions in the boundary layer are given by r and θ, respectively. The important length scales are the local heating length $R\theta$ and the local boundary layer thickness δ, whereas the important velocity scales are the local liquid and vapor velocities, u_ℓ and u_g, respectively. The latter two quantities are defined for the local velocities in the direction parallel to the curved heating surface. Under the influence of gravity, the buoyancy force driving the two-phase motion is proportional to $\alpha(\rho_\ell-\rho_g)g\sin\theta$, where α is the local void fraction of the two-phase mixture and $g\sin\theta$ is the local acceleration of gravity in the direction parallel to the heating surface.

According to Cheung and Epstein [14], the momentum relation for the vapor–liquid mixture in the two-phase boundary layer is governed by the following differential equation applicable to any location θ along the hemispherical heating surface:

$$\frac{d}{d\theta}\{[\rho_g\alpha u_g^2+\rho_\ell(1-\alpha)u_\ell^2]\delta\sin\theta\} = \alpha\delta Rg(\rho_\ell-\rho_g)\sin^2\theta-(\tau_w+\tau_i)R\sin\theta \quad (18)$$

where τ_w and τ_i are the wall and the interfacial shear stresses. These quantities are given by [14]:

$$\tau_w+\tau_i = 0.5C_f[\alpha u_g+(1-\alpha)u_\ell][\rho_g\alpha u_g+\rho_\ell(1-\alpha)u_\ell] \quad (19)$$

where C_f is a friction coefficient having the value of 0.005.

A mass balance on the liquid phase across the thickness of the two-phase boundary layer at any location θ gives

$$\frac{d}{d\theta}[(1-\alpha)u_\ell\delta\sin\theta] = j_\ell R\sin\theta \quad (20)$$

where j_ℓ is the net liquid velocity entrained from the ambient fluid into the two-phase boundary layer at θ. Physically, the quantity j_ℓ represents the 'entrained' component of the liquid mass swept into the boundary layer by the two-phase motion, excluding the 'suction' component of the liquid mass due to liquid depletion by boiling on the heating surface. A detailed description of the quantity j_ℓ will be given in the Results and Discussion section. Similarly, a mass balance on the vapor phase across the thickness of the two-phase boundary layer under saturated boiling conditions at any location θ gives

$$\frac{d}{d\theta}[\alpha u_g\delta\sin\theta] = \frac{q''_{CHF}R\sin\theta}{\rho_g h_{fg}} \quad (21)$$

where in deriving the above expression, the local wall heat flux on the heating surface has been assumed equal to the local critical heat flux. This corresponds to the critical heating condition for which the local CHF limit is reached in all upstream locations on the outer surface of the hemispherical vessel. This situation gives rise to the maximum local vapor velocity and boundary layer thickness that can possibly be attained at a given downstream location θ. Physically, the use of q''_{CHF} in equation (21) is consistent with the notion that CHF represents the upper bound of the excellent state of nucleate boiling. Beyond this upper limit, dryout will occur on the heating surface.

To close the governing system, an independent expression is needed for the relative velocity between the liquid and vapor phases. This is obtained by assuming that once the vapor mass departs from the heating surface, it would attain its terminal rise velocity relative to the liquid phase in the two-phase boundary layer. It follows that [15]

$$u_g = u_\ell+1.53\left[\frac{\sigma g\sin\theta(\rho_\ell-\rho_g)}{\rho_\ell^2}\right]^{1/4} \quad (22)$$

where $g\sin\theta$ represents the local gravitational force tangential to the heating surface. As will be seen in the numerical solution, the relative velocity is important only in the upstream locations near the bottom center. In most downstream locations, the relative velocity is considerably smaller than the vapor and liquid velocities themselves. This is owing to the fact that the vapor generation rate is extremely high at the CHF limit, resulting in very large vapor and liquid velocities in the two phase boundary layer. Thus any errors associated with the relative velocity used in equation (22) will not materially affect the predicted boundary layer flow behavior.

Inspection of equations (17)–(22) indicates that the following local boundary layer variables, namely, the dimensionless critical heat flux, Q_{CHF}, dimensionless boundary layer thickness, Δ, dimensionless vapor velocity, U_g, and dimensionless liquid velocity, U_ℓ, can be introduced to simplify the governing system:

$$q''_{CHF} = \rho_g h_{fg}\left[\frac{\sigma g(\rho_\ell-\rho_g)}{\rho_g^2}\right]^{1/4}\left(1+\frac{\rho_g}{\rho_\ell}\right)^{1/3} Q_{CHF} \quad (23a)$$

$$\delta = \left[\frac{\sigma R^2}{g(\rho_\ell-\rho_g)}\right]^{1/4}\left(\frac{\rho_g}{\rho_\ell}\right)^{-0.1}\Delta \quad (23b)$$

$$u_g = \left[\frac{Rg(\rho_\ell-\rho_g)}{\rho_g}\right]^{1/2}\left(\frac{\rho_g}{\rho_\ell}\right)^{0.1} U_g \quad (23c)$$

$$u_\ell = \left[\frac{Rg(\rho_\ell-\rho_g)}{\rho_\ell}\right]^{1/2} U_\ell. \quad (23d)$$

In terms of the dimensionless local variables, equations (17)–(22) can be written as

$$Q_{CHF} = B(U_\ell/\Delta_0)^{1/3} \quad (24)$$

$$\frac{\mathrm{d}}{\mathrm{d}\theta}\left\{\left[\alpha U_g^2+\left(\frac{\rho_g}{\rho_\ell}\right)^{-0.2}(1-\alpha)U_\ell^2\right]\Delta\sin\theta\right\}$$

$$=\alpha\Delta\sin^2\theta\left(\frac{\rho_g}{\rho_\ell}\right)^{-0.2}-0.5C_f L_b^{-1/2}\left(\frac{\rho_g}{\rho_\ell}\right)^{0.1}$$

$$\times\sin\theta\left[\alpha U_g+\left(\frac{\rho_g}{\rho_\ell}\right)^{-0.6}(1-\alpha)U_\ell\right]$$

$$\left[\alpha U_g+\left(\frac{\rho_g}{\rho_\ell}\right)^{0.4}(1-\alpha)U_\ell\right] \quad (25)$$

$$\frac{\mathrm{d}}{\mathrm{d}\theta}[(1-\alpha)U_\ell\Delta\sin\theta]=J_\ell\left(\frac{\rho_g}{\rho_\ell}\right)^{0.1}L_b^{-1/2}\sin\theta \quad (26)$$

$$\frac{\mathrm{d}}{\mathrm{d}\theta}[\alpha U_g\Delta\sin\theta]=Q_{\mathrm{CHF}}\sin\theta \quad (27)$$

$$U_\ell=\left(\frac{\rho_g}{\rho_\ell}\right)^{-0.4}U_g-1.53(L_b^2\sin\theta)^{1/4} \quad (28)$$

where

$$\Delta_0=\left[\frac{\sigma R^2}{g(\rho_\ell-\rho_g)}\right]^{-1/4}\left(\frac{\rho_g}{\rho_\ell}\right)^{0.1}\delta_0 \quad (29)$$

$$J_\ell=\left[\frac{Rg(\rho_\ell-\rho_g)}{\rho_\ell}\right]^{-1/2}j_\ell \quad (30)$$

$$L_b=\frac{1}{R}\left[\frac{\sigma}{g(\rho_\ell-\rho_g)}\right]^{1/2}. \quad (31)$$

Physically, the dimensionless parameter L_b represents the length ratio between the intrinsic bubble size and the vessel radius.

Initial conditions and the universal constant

It remains necessary to determine the initial value, Δ_0, for the dimensionless boundary layer thickness. This requires considerations of the vapor mass that forms in the bottom center region of the heated vessel. Based upon the vapor dynamics observed in refs. [8, 9], the aspect ratio of the vapor mass is very close to four, i.e. $C_4 = 4$ in equation (14). The vapor velocity, u_{g_0}, at an initial location θ_0 near the bottom center can be determined from a mass balance, i.e.

$$\rho_g u_{g_0}\alpha(2\pi R\delta_0\sin\theta_0)=\frac{1}{h_{fg}}\int_0^{\theta_0}q''_{\mathrm{CHF}}2\pi R^2\sin\theta\,\mathrm{d}\theta. \quad (32)$$

Since $\theta_0 \ll 1$, the local critical heat flux can be treated as a constant equal to $(q''_{\mathrm{CHF}})_0$. An expression for u_{g_0}, may thus be obtained by carrying out the integration in equation (32). The result is

$$u_{g_0}=\frac{(q''_{\mathrm{CHF}})_0}{\alpha\rho_g h_{fg}}\left[\frac{1-\cos\theta_0}{\sin\theta_0}\right]\left(\frac{R}{\delta_0}\right). \quad (33)$$

For $\theta_0 \ll 1$, it can be shown that

$$\sin\theta_0=\theta_0 \quad \text{and} \quad \cos\theta_0=1-\tfrac{1}{2}\theta_0^2. \quad (34)$$

Substituting equation (34) into equation (33), the following expression is obtained for u_{g_0},

$$u_{g_0}=\frac{(q''_{\mathrm{CHF}})_0}{\alpha\rho_g h_{fg}}\left(\frac{R}{\delta_0}\right)\frac{\theta_0}{2}. \quad (35)$$

In terms of the dimensionless quantities, equation (35) can be written as

$$U_{g_0}=\frac{(Q_{\mathrm{CHF}})_0}{\alpha\Delta_0}\frac{\theta_0}{2} \quad (36)$$

where U_{g_0} and $(Q_{\mathrm{CHF}})_0$ are the initial values of U_g and Q_{CHF} at $\theta = \theta_0$. From equations (28) and (34), the dimensionless liquid velocity at θ_0 is given by

$$U_{\ell_0}=\left(\frac{\rho_g}{\rho_\ell}\right)^{-0.4}\frac{(Q_{\mathrm{CHF}})_0}{\alpha\Delta_0}\frac{\theta_0}{2}-153L_b^{1/2}\theta_0^{1/4}. \quad (37)$$

Applying equation (24) at $\theta = \theta_0$ and using equation (37), an implicit relationship can be derived for Δ_0. This is

$$\left(\frac{\rho_g}{\rho_\ell}\right)^{-0.4}\frac{(Q_{\mathrm{CHF}})_0}{\alpha\Delta_0}\frac{\theta_0}{2}-1.53L_b^{1/2}\theta_0^{1/4}=\left[\frac{(Q_{\mathrm{CHF}})_0}{B}\right]^3\Delta_0. \quad (38)$$

Assuming the boundary-layer flow quantities to be nearly constant over the bottom-center region where $0 \leqslant \theta \leqslant \theta_0$ and that $\mathrm{d}\Delta/\mathrm{d}\theta = 0$ at $\theta = \theta_0$, equation (25) can be integrated to give

$$\alpha U_{g_0}^2+\left(\frac{\rho_g}{\rho_\ell}\right)^{-0.2}(1-\alpha)U_{\ell_0}^2$$

$$=\frac{\alpha\theta_0^2}{3}\left(\frac{\rho_g}{\rho_\ell}\right)^{-0.2}-0.25C_f L_b^{-1/2}\left(\frac{\rho_g}{\rho_\ell}\right)^{0.1}\theta_0\left[\alpha U_{g_0}\right.$$

$$\left.+\left(\frac{\rho_g}{\rho_\ell}\right)^{-0.6}(1-\alpha)U_{\ell_0}\right]\left[\alpha U_{g_0}+\left(\frac{\rho_g}{\rho_\ell}\right)^{0.4}(1-\alpha)U_{\ell_0}\right] \quad (39)$$

where equation (34) has been employed in deriving the above equation. The value of Δ_0 can be determined iteratively from equations (36)–(39). Once Δ_0 is known, equations (24)–(28) can be solved simultaneously to determine the spatial variation of Q_{CHF}.

The above formulation results in one universal constant that needs to be determined from experimental data. To do this, the vapor dynamic and the local CHF limit at $\theta = \theta_0$ observed in [8–10] are employed. The criterion for the occurrence of the local CHF limit in the bottom center region is based on the depletion of the liquid film in the micro-layer before the departure of the vapor mass from the heating surface. The mass of the liquid film is $\rho_\ell\delta_m(A_w-A_v)$ whereas the total rate of nucleate boiling heat transfer is $q''_{\mathrm{NB}}A_w$. If the duration of the vapor ejection cycle is Δt_v, then local dryout would occur if $q''_{\mathrm{NB}}A_w\Delta t_v/h_{fg}$ becomes equal to or larger than the mass of the liquid film. Thus the local CHF limit is given by

$$(q''_{\rm CHF})_0 = \frac{1}{A_{\rm w}\Delta t_{\rm v}}[\rho_\ell(\delta_{\rm m})_{\rm CHF}(A_{\rm w}-A_{\rm v})h_{\rm fg}]$$

$$= \frac{\rho_\ell h_{\rm fg}(\delta_{\rm m})_{\rm CHF}}{\Delta t_{\rm v}} \quad (40)$$

where the term involving the area ratio has been ignored as $A_{\rm v}/A_{\rm w} \ll 1$. Substituting equation (16) into equation (40) and rearranging, an expression for the universal constant can be derived. This is

$$C_3 = \frac{\Delta t_{\rm v}}{\sigma\rho_\ell\rho_{\rm g}}\left(1+\frac{\rho_{\rm g}}{\rho_\ell}\right)^{-1}\left(\frac{\rho_{\rm g}}{\rho_\ell}\right)^{-0.4}\left[\frac{(q''_{\rm CHF})_0}{h_{\rm fg}}\right]^3. \quad (41)$$

In refs. [8, 9], the duration $\Delta t_{\rm v}$, was found to be 0.25 s whereas the local CHF limit was 0.4 MW m^{-2}. Using the properties for water at one atmospheric pressure, i.e. $\sigma = 0.0588$ N m^{-1}, $\rho_\ell = 958$ kg m^{-3}, $\rho_{\rm g} = 0.598$ kg m^{-3}, and $h_{\rm fg} = 2.257$ MJ kg^{-1}, the value of C_3 is calculated to be 0.00079. It follows that the universal constant in equations (24) and (38) is given by

$$B = (C_3/C_4)^{1/3} = 0.0582 \quad (42)$$

where the value of $C_4 = 4$ has been used.

RESULTS AND DISCUSSION

Spatial variation of the critical heat flux

Equations (24)–(28) form a complete set of coupled equations governing the local variations of the critical heat flux, $Q_{\rm CHF}$, the vapor and liquid velocities $U_{\rm g}$ and U_ℓ, respectively, the boundary layer thickness, Δ, and the void fraction, α. To solve this set of equations, however, input information is needed for the liquid entrainment rate, J_ℓ in equation (26). Unfortunately, no experimental evidence on the liquid entrainment is available to date. To circumvent this difficulty, it is postulated that the local void fraction in the two-phase boundary layer assumes a constant value as the CHF limit is approached on the heating surface. This postulation, which is consistent with the experimental observation of Cheung and Haddad [8, 9], will be justified from a theoretical point of view in the next section. By setting α equal to 0.915 according to the experimental data of Cheung and Haddad [8, 9], equation (26) which contains the liquid entrainment term, can be eliminated from the governing system. The remaining unknown quantities (i.e. $Q_{\rm CHF}$, $U_{\rm g}$, U_ℓ and Δ) can readily be determined from equations (24), (25), (27) and (28).

Based upon the constant-void-fraction postulation, calculations of the local boundary layer flow quantities and the local CHF limits have been made over the range of $0 \leqslant \theta \leqslant \pi/2$ for water. In these calculations, the value of $L_{\rm b}$ has been set equal to 0.164, 0.0164, 0.00164 and 0.000164, corresponding respectively to a diameter of 1.2 in (0.0305 m), 12 in (0.305 m), 120 in (3.05 m), and 1200 in (305 m) for the heated hemispherical vessel under consideration. Results are shown in Figs. 3–6. For all values of $L_{\rm b}$, the boundary layer thickness increases considerably from the bottom center to the upper edge of the vessel (see Fig. 3). However, the dimensionless boundary layer thickness is a weak function of the physical size of the vessel. The size effect is important only when the vessel diameter is very small. The actual boundary layer thickness, on the other hand, is a strong function of $L_{\rm b}$. For $L_{\rm b} < 0.05$, however, δ is almost inversely proportional to the square root of $L_{\rm b}$. Thus for vessels larger than 0.1 m in diameter, δ would vary according to the square root of the vessel diameter, whereas Δ is essentially independent of the vessel size.

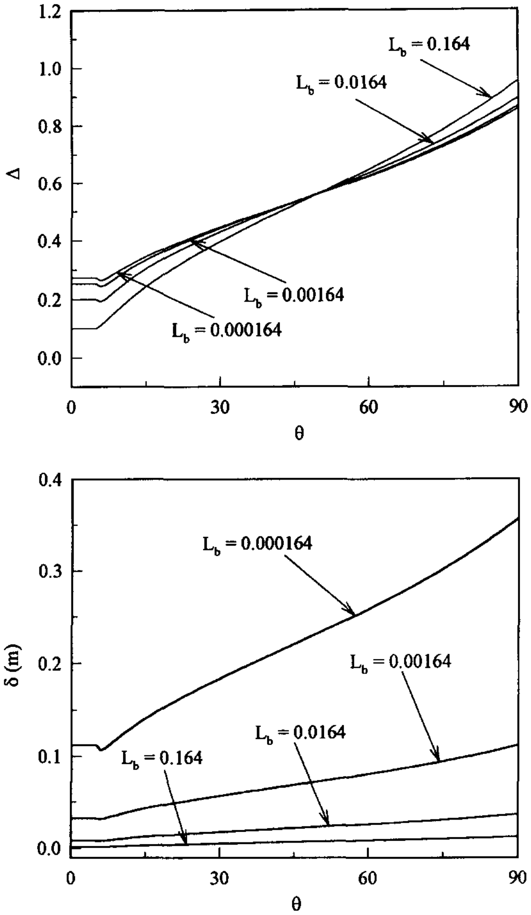

Fig. 3. Spatial variation of the local thickness of the two-phase boundary layer.

The spatial variations of the vapor and liquid velocities are presented in Figs. 4 and 5. For all values of $L_{\rm b}$, the vapor and liquid velocities increase by more than an order of magnitude from the bottom center to the upper edge of the vessel. The relative velocity between the liquid and vapor phases is on the same order of the vapor and liquid velocities when θ is small. For large values of θ, the relative velocity is an order of magnitude smaller than the liquid and vapor

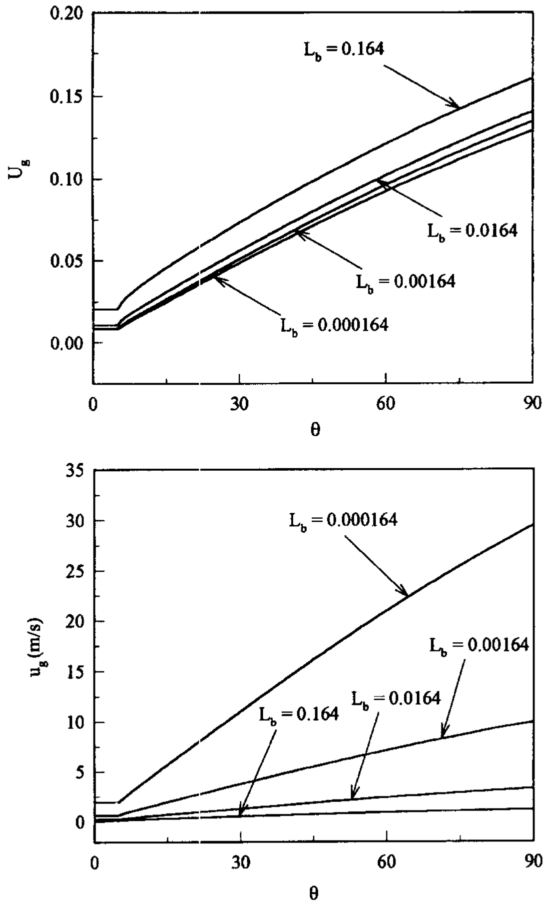

Fig. 4. Spatial variation of the local vapor velocity in the two-phase boundary layer.

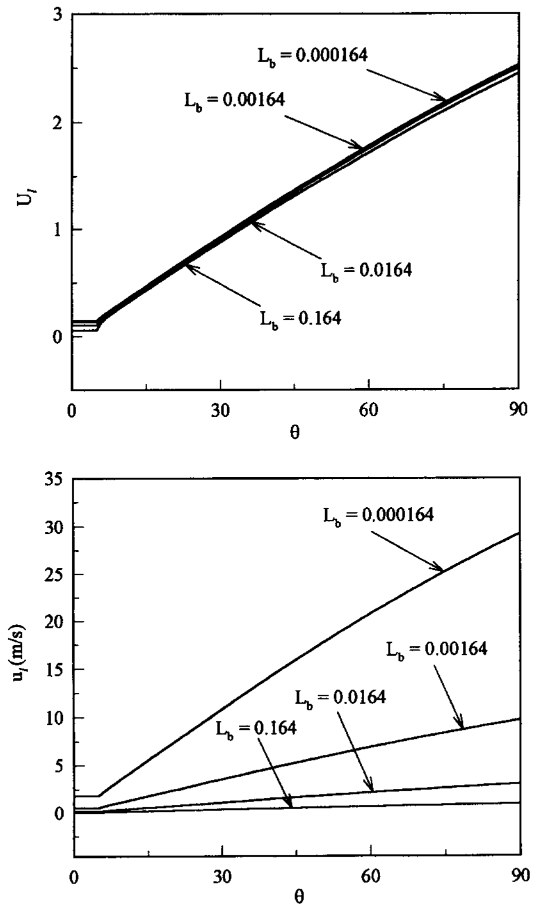

Fig. 5. Spatial variation of the local liquid velocity in the two-phase boundary layer.

velocities. The effect of L_b is quite strong on u_ℓ and u_g, but very weak on the dimensionless quantities U_ℓ and U_g. For $L_b < 0.05$, both u_ℓ and u_g are almost inversely proportional to the square root of L_b. Thus for vessels larger than 0.1 m in diameter, u_ℓ and u_g would vary according to the square root of the vessel diameter whereas U_ℓ and U_g are essentially independent of the vessel size.

Figure 6 shows the spatial variations of the dimensionless critical heat flux and the actual critical heat flux. Both Q_{CHF} and q''_{CHF} are weak functions of the size parameter L_b for cases of L_b equal to or less than 0.0164. This clearly demonstrates the fact that for heated vessels with diameters considerably larger than the characteristic bubble size, the critical heat flux is weakly dependent on the vessel size. As shown in equation (17), the local critical heat flux is given by the 1/3 power of the ratio between the local liquid velocity and the local boundary layer thickness. For $L_b < 0.05$, both u_ℓ and δ vary according to the square root of the vessel diameter. Thus the size effect on u_ℓ and δ_0 cancels out and q''_{CHF} becomes almost independent of L_b. Note that the local critical heat flux increases by more than 100% from the bottom center to the upper edge of the vessel. This result is similar to the spatial variations of CHF observed experimentally by Cheung and Haddad [9], Haddad *et al.* [10] and Theofanous *et al.* [12]. However, it is opposite to the CHF variation observed by El-Genk and Glebov [11]. Physically, this is because of the two-phase boundary layer flow effect, which was present in the experiments by Cheung and Haddad [9], Haddad *et al.* [10] and Theofanous *et al.* [12] but not present in the transient experiments by El-Genk and Glebov [11]. In the latter case the heating surface was too small ($\sim$50 mm) for a two-phase boundary layer to develop. For the downward facing heating surface under consideration, the local liquid velocity increases by more than an order of magnitude over the range of $0 \leqslant \theta \leqslant \pi/2$. As a result, there is a large increase in the local liquid supply rate, resulting in a significant spatial variation of the critical heat flux.

Liquid entrainment and the constant-void-fraction postulation

The results presented in the previous section were based on the postulation that the local void fraction assumes a constant value as the CHF limit is approached on the heating surface. Although the constant-void-fraction postulation is consistent with the experimental observation of Cheung and Haddad [8,

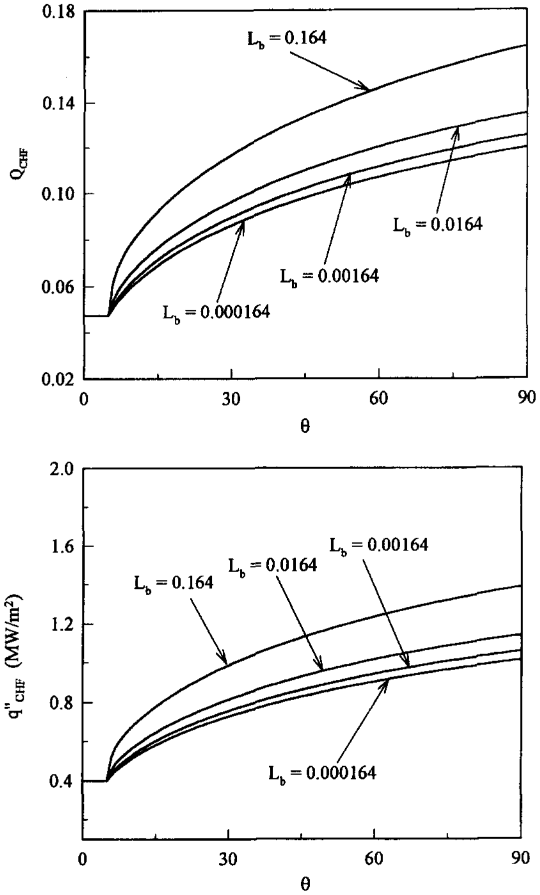

Fig. 6. Spatial variation of the local critical heat flux on the heating surface.

9], it is necessary to justify the postulation from a theoretical point of view. To do this, an expression is needed for the liquid entrainment j_ℓ in equation (20). Experimental measurements of entrainment with turbulent gas jets having a density different than the ambient fluid have been performed by Ricou and Spalding [16]. They found that the entrainment velocity, j_ℓ, is proportional to the mean velocity u_j of the jet as well as the square root of the ratio of the density ρ_j of the jet to the density ρ_∞ of the ambient fluid, e.g.

$$j_\ell = E_0 u_j \left(\frac{\rho_j}{\rho_\infty}\right)^{1/2} \tag{43}$$

where the proportionality constant E_0 is the so-called 'entrainment coefficient'. By extending the finding of Ricou and Spalding [16] to the two-phase boundary layer under consideration, the following expressions can be written:

$$u_j = \alpha u_g + (1-\alpha)u_\ell \quad \text{and} \quad \frac{\rho_j}{\rho_\infty} = \frac{\alpha\rho_g + (1-\alpha)\rho_\ell}{\rho_\ell \sin\theta} \tag{44}$$

where the term $\sin\theta$ is included in the denominator of the density ratio to account for the downward facing orientation of the heating surface. Whereas the turbulent jets studied by Ricou and Spalding [16] are vertically oriented, the two-phase boundary layer under consideration is inclined along the heating surface. The component of the gravity force parallel to the flow is given by $g\sin\theta$. Physically the second expression in equation (44) represents the ratio of the body force acting on the two phase mixture to that acting on the ambient fluid. From equations (43) and (44), an expression for the liquid entrainment from the ambient fluid to the two-phase boundary layer can be obtained. This is

$$j_\ell = E_0[\alpha u_g + (1-\alpha)u_\ell]\left[\frac{\alpha\rho_g + (1-\alpha)\rho_\ell}{\rho_\ell \sin\theta}\right]^{1/2}. \tag{45}$$

The above expression can be viewed as the two-phase version of the expression proposed by Morton [17] for turbulent jets driven by buoyancy. A similar expression has also been employed by Cheung and Epstein [14] to study the behavior of a two-phase boundary layer on inclined flat surfaces. Substituting equations (30) and (45) into equation (26), the following dimensionless liquid continuity equation can be obtained:

$$\frac{d}{d\theta}[(1-\alpha)U_\ell \Delta \sin\theta] = E_0 \sin^{1/2}\theta \left(\frac{\rho_g}{\rho_\ell}\right)^{0.1} L_b^{-1/2}\left[\left(\frac{\rho_g}{\rho_\ell}\right)^{-0.4}\alpha U_g + (1-\alpha)U_\ell\right]\left[\frac{\alpha\rho_g + (1-\alpha)\rho_\ell}{\rho_\ell}\right]^{1/2}. \tag{46}$$

Calculations of the local boundary layer flow quantities and the local CHF limits have been made by solving equations (24), (25), (27), (28) and (46) for water, treating the local void fraction α as an unknown quantity. In these calculations, the value of L_b has been fixed at 0.0164, corresponding to a vessel diameter of 12 in (0.305 m), which is the same as the vessel size employed in the experimental work of Cheung and Haddad [8, 9]. Meanwhile, various values have been assumed for the entrainment coefficient by setting E_0 equal to 0.116 C_5, where C_5 is a constant factor having a value varying from 0.5 to 1.0. The value of $C_5 = 1.0$ (i.e. $E_0 = 0.116$) has been used by Morton [17] for turbulent jets and by Cheung and Epstein [14] for two-phase boundary layer flows. In the present case, however, E_0 is expected to be smaller than 0.116 because of the configuration of the downward facing curved heating surface and the wall effect on liquid entrainment. For all values of $0.5 \leqslant C_5 \leqslant 1.0$ employed in the calculations, the local void fraction was found to be nearly constant over the length of the hemispherical heating surface. Results for two special

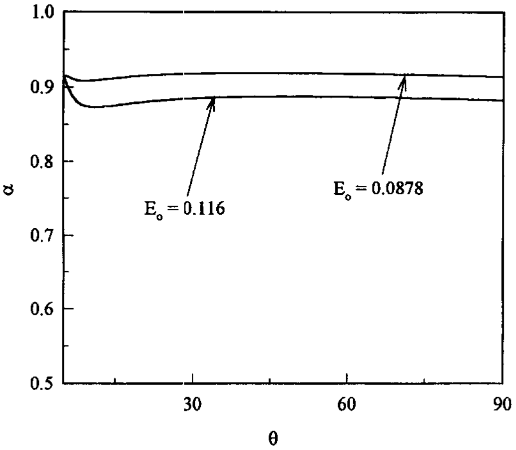

Fig. 7. The predicted local void fraction profiles in the two-phase boundary layer.

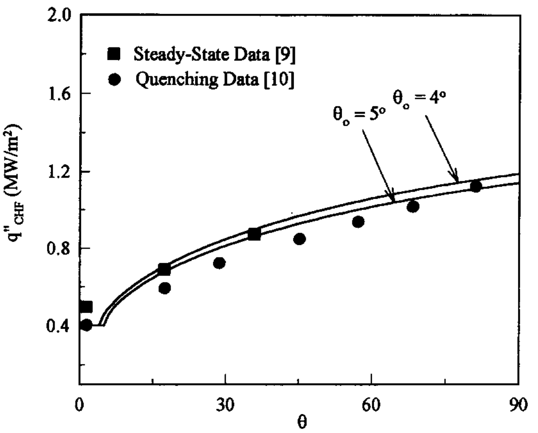

Fig. 8. Comparison of the predicted critical heat fluxes with experimental data.

cases are presented in Fig. 7. For the case of $E_0 = 0.116$ (i.e. $C_5 = 1.0$), the local void fraction is bounded within $\pm 2.5\%$ of 0.892, whereas for the case of $E_0 = 0.0878$ (i.e. $C_5 = 0.75$) α is bounded within $\pm 0.5\%$ of 0.915. These results clearly indicate that the constant-void-fraction postulation is a valid approach as it complies with the conservation of liquid mass, i.e. the liquid continuity equation. Based on the value of $\alpha = 0.915$ observed in the experimental work of Cheung and Haddad [8, 9], the entrainment coefficient for the present two-phase boundary layer flow is determined to be $E_0 = 0.0878$.

Comparison with experiments

The initial values of the boundary layer quantities employed in the present work are treated as constant throughout the bottom center region of the hemispherical vessel where $0 \leqslant \theta \leqslant \theta_0$. This treatment is consistent with the experimental observation of Cheung and Haddad [8, 9] where a single large elongated vapor mass was always found present in the bottom center region. For a given value of L_b, the initial location θ_0 is determined by numerical iteration from equations (36)–(39). It is found that for L_b much less than unity θ_0 is a weak function of L_b having a value approximately equal to 4.5°. This value is very close to the one obtained experimentally based on the observed vapor size at the bottom center. For the purpose of comparison, results obtained for θ_0 equal to 4° and 5° are shown in Fig. 8 along with the CHF data of Haddad *et al.* [10] from quenching experiments and Cheung and Haddad [9] from steady-state measurements. Relative to the case of $\theta_0 = 5°$, the CHF value predicted for the case of $\theta_0 = 4°$ is slightly higher. However, the differences are well within the scatter of the experimental data. More importantly, the same trend (i.e. the same spatial variation) is predicted for the critical heat flux, independent of the initial location θ_0. Apparently, the CHF variation is not sensitive to the value of θ_0. In both cases, the predicted spatial variations of the critical heat flux are found to compare reasonably well with the experimental data.

CONCLUSIONS

A hydrodynamic CHF model has been developed for saturated pool boiling on the outer surface of a heated hemispherical vessel. The model represents the first attempt to discern the spatial variation of the critical heat flux in pool boiling. Based upon the results of this study, the following conclusions can be made:

(1) For nucleate boiling on a downward facing hemispherical surface, there is a micro-layer underneath each elongated vapor slug growing on the surface. Local dryout of the surface occurs when the local rate of liquid supply to the micro-layer becomes smaller than the rate of depletion of the liquid film by boiling. This critical condition determines the maximum wall heat flux corresponding to the local CHF limit.

(2) One salient feature of the present problem is the formation of an external buoyancy-driven two-phase liquid/vapor boundary layer flow on the heating surface. Because of the two-phase boundary layer, the local rate of liquid supply increases significantly from the bottom center to the upper edge of the vessel, thus greatly enhancing the local CHF limit. This provides a physical explanation for the large spatial variation of the critical heat flux observed experimentally by Cheung and Haddad [8, 9] and Haddad *et al.* [10]. Evidently, for downward facing surfaces, the critical heat flux cannot be assumed uniform over the entire heating surface.

(3) For hemispherical vessels with diameters considerably larger than the characteristic bubble size, both the local liquid supply rate and the local boundary layer thickness are approximately proportional to the square root of the vessel diameter. Since the critical heat flux depends only on the ratio of the liquid supply rate to the boundary layer thickness, the size effect

tends to cancel out altogether. As a result, the critical heat flux is almost independent of the physical size of the vessel.

(4) Based upon the argument that the liquid entrainment is proportional to the square root of the ratio of the body force acting upon the two-phase mixture to that on the ambient fluid, an analytical expression is obtained for the liquid velocity entrained from the ambient fluid to the two-phase boundary layer. Using this analytical expression in the liquid continuity equation, an approximately constant void fraction is predicted in the two-phase boundary layer as the CHF limit is approached on the heating surface. This predicted result is consistent with the experimental observation of Cheung and Haddad [8, 9]. Additional experimental evidence, however, is needed to confirm the range of validity of the liquid entrainment expression.

Acknowledgements—This work was sponsored by the U.S. Nuclear Regulatory Commission under contract no. NRC-04-93-061.

REFERENCES

1. Katto, Y., Critical heat flux. *Advances in Heat Transfer*, 1985, **17,** 1–65.
2. Carey, V. P., *Liquid-Vapor Phase Change Phenomenon*. Hemisphere, New York, 1992.
3. Kutateladze, S. S., On the transition to film boiling under natural convection. *Kotloturbostroenie*, 1948, **3,** 10–15.
4. Zuber, N., Hydrodynamics aspects of boiling heat transfer. AEC report, AECU-4439, 1959.
5. Lienhard, J. H. and Dhir, V. K., Hydrodynamic predictions of peak pool-boiling heat fluxes from finite bodies. *Transactions of the American Society of mechanical Engineers, Series C, Journal of Heat Transfer*, 1973, **95,** 152–158.
6. Lienhard, J. H. and Hasan, M., On predicting boiling burnout with the mechanical energy stability criterion. *Transactions of the American Society of Mechanical Engineers, Series C, Journal of Heat Transfer*, 1979, **101,** 276–279.
7. Haramura, Y. and Katto, Y., A new hydrodynamic model of critical heat flux, applicable widely to both pool and forced convection boiling on submerged bodies in saturated liquids. *International Journal of Heat and Mass Transfer*, 1983, **26,** 389–399.
8. Cheung, F. B. and Haddad, K. H., Observation of the dynamic behavior of the two-phase boundary layers in the SBLB experiments. *Proceedings of the Twenty-Second Water Reactor Safety Meeting*, Vol. 2. Washington, DC, 1994, pp. 87–112.
9. Cheung, F. B. and Haddad, K. H., Steady-state observations of critical heat flux phenomenon on a downward facing hemispherical surface. *Proceedings of the Twenty Third Water Reactor Safety Meeting*, Washington, DC 1995.
10. Haddad, K. H., Liu, Y. C. and Cheung, F. B., Spatial variation of critical heat flux on a downward facing hemispherical surface. *Proceedings of the Thirtieth National Heat Transfer Conference*, HTD-Vol. 316. Washington DC, 1995, pp. 23–32.
11. El-Genk, M. S. and Glebov, A. G., Transient pool boiling from downward facing curved surfaces, *International Journal of Heat and Mass Transfer*, 1995, **38,** 2209–2224.
12. Theofanous, T. G., Syri S., Salmassi, T., Kymalainen, O. and Tuomisto, H., Critical heat flux through curved downward facing, thick walls. *Nuclear Engineering and Design*, 1994, **151,** 247–258.
13. Chu, T. Y., Bentz, J. H. and Simpson, R. B., Observation of the boiling process from a large downward facing torispherical surface. *Proceedings of the Thirtieth National Heat Transfer Conference*, Washington, DC 1995.
14. Cheung, F. B. and Epstein, M., Two-phase gas bubble-liquid boundary layer flow along vertical and inclined surfaces. *Nuclear Engineering and Design*, 1987, **99,** 93–100.
15. Wallis, G. B., *One-Dimensional Two-Phase Flow*. McGraw-Hill, New York, 1969.
16. Ricou, F. P. and Spalding, D. B., Measurements of entrainment of axisymmetrical turbulent jets. *Journal of Fluid Mechanics*, 1961, **11,** 21–32.
17. Morton, B. R., Modeling fire plumes. *Tenth Symposium On Combustion*. The Combustion Institute, 1965, pp. 973–986.